Jianhang Chen
Chinese Academy of Sciences,
Institute of Metal Research,
72 Wenhua Road,
Shenyang 110016, China;
School of Materials Science and Engineering,
University of Science and Technology of China,
72 Wenhua Road,
Shenyang 110016, China
e-mail: jhchen18s@imr.ac.cn

Siyang Gao[1]
Chinese Academy of Sciences,
Institute of Metal Research,
72 Wenhua Road,
Shenyang 110016, China
e-mail: sygao@imr.ac.cn

Peng Wang
Chinese Academy of Sciences,
Institute of Metal Research,
72 Wenhua Road,
Shenyang 110016, China
e-mail: chenjhchn@163.com

Weihai Xue
Chinese Academy of Sciences,
Institute of Metal Research,
72 Wenhua Road,
Shenyang 110016, China
e-mail: whxue@imr.ac.cn

Shu Li
Chinese Academy of Sciences,
Institute of Metal Research,
72 Wenhua Road,
Shenyang 110016, China
e-mail: shuli@imr.ac.cn

Deli Duan[1]
Chinese Academy of Sciences,
Institute of Metal Research,
72 Wenhua Road,
Shenyang 110016, China;
School of Materials Science and Engineering,
University of Science and Technology of China,
72 Wenhua Road,
Shenyang 110016, China
e-mail: duandl@imr.ac.cn

Study on Tribological Behavior of Zinc Phosphate Impregnated Graphite Under Oil Lubrication Condition

The tribological behavior of zinc phosphate impregnated graphite (ZPIG) against nickel-based superalloy (GH4169) in oil environment was investigated, and the lubrication and wear mechanism were also determined in this study. Tribological tests were run under different tribological conditions using a ring-on-disk device. The results showed that, under any load conditions, zinc phosphate impregnated graphite had the lowest coefficient of friction (COF) and wear-rate at 200 rpm. Under the identical rotating speed condition, the minimum coefficient of friction and wear-rate were obtained when the load was 500 N and 1000 N. The lubrication mechanism, which could be reflected by the transfer layer of friction counterpart, was related to the coefficient of friction, wear-rate, and oil temperature to affect contact characteristics of two solid surfaces and formation ability of liquid film. The wear mechanism of zinc phosphate impregnated graphite under oil lubrication conditions was dominated by abrasive wear and material removal was achieved through the fracture mechanism. [DOI: 10.1115/1.4051586]

Keywords: zinc phosphate impregnated graphite, oil lubrication, tribological behavior, lubrication mechanism, wear mechanism

1 Introduction

Graphite materials have been widely used in mechanical seals field because of their self-lubricating properties, good chemical stability, and corrosion resistance [1–4]. However, traditional graphite materials have high porosity and poor airtightness. The presence of pores usually lead to low mechanical strength and poor tribological behavior, which makes traditional graphite difficult to use as sealing materials directly [5]. Therefore, graphite materials have been impregnated with inorganic salt [6–8], resin [3,9], or molten metal [10,11] to block the pores to improve their mechanical properties and tribological performances.

For a long time, the tribological behavior of graphite materials has been a hot research topic. The early studies mainly focused on the friction reduction mechanism of traditional graphite materials. Bernel [12], Bragg [13], and Bryant et al. [14] attributed the low friction and wear characteristics of graphite to the lamellar structure and weak van der Waals forces between layers. Savage [15] and Savage and Schaefer [16] found that slipperiness of graphite materials depended on the surface adsorption films, especially water, which could cover the carbon atoms and provide surfaces of low cohesion, thereby reducing the wear of graphite materials. Bollmann and Spreadborough [17] and Spreadborough [18] found as the graphite materials were rubbed, the packets of graphite planes would be rolled up to form small roller bearings to reduce the coefficient of friction (COF). Clark and Lancaster [19], Lancaster [20],

[1]Corresponding authors.

Contributed by the Tribology Division of ASME for publication in the Journal of Tribology. Manuscript received March 14, 2021; final manuscript received June 22, 2021; published online July 16, 2021. Assoc. Editor: Wenyang Zhang.

and Jones [21,22] found that graphite would form a complete transfer film on the surface of the counterparts to reduce the coefficient of friction and wear volume. The transfer film, which was the third phase with low shear strength, protected the graphite itself through the balance of the destruction and regeneration.

At present, the research focus is mainly transferred to the tribological behavior of impregnated graphite [3,4,23–25]. Zhu et al. [3] compared the tribological performance of impregnated and nonimpregnated graphite under dry friction conditions. He founded that the addition of furan resin would help to form a stable lubricating transfer film and therefore reduce the coefficient of friction. Zhang et al. [23,24] studied the friction characteristics of phenolic resin impregnated graphite and nonimpregnated graphite in dry, oil, and water environments. He found that impregnated graphite exhibited better tribological performance under lubrication conditions, and it could maintain a stable tribological state under high PV value. Zhao et al. [25] mainly studied the tribological properties of furan resin impregnated graphite at different friction temperatures and found that the tribological performance increased significantly with the raise of friction temperature.

From the above, it can be seen that the existing work of tribological behavior mainly focus on the traditional and resin impregnated graphite materials. However, for zinc phosphate impregnated graphite (ZPIG), which has been applied in engineering practice of aeroengines, there are few reports on its tribological characteristics.

Therefore, the purpose of this paper is to study the tribological behavior of zinc phosphate impregnated graphite and focus on the influence of load, rotating speed under oil lubrication conditions. The typical lubrication and wear mechanism of zinc phosphate impregnated graphite are analyzed and discussed. The significance of this study provides insight into the tribological behavior of impregnated zinc phosphate graphite under different tribological conditions and an important basis for selecting suitable working conditions for reference.

Table 1 Mechanical and physical parameters of ZPIG and GH4169

Material	Density (g/cm^3)	Young's modulus (GPa)	Thermal conductivity (W/(m · K))	Hardness	Porosity (vol%)
ZPIG	1.8	20.5	80	85 HS	7.0
GH4169	8.24	199.9	14.7	380 HBS	–

2 Material and Experiment

2.1 Material. Zinc phosphate impregnated graphite and Nickel-based superalloy (GH4169) were used as the friction pair in the present work. ZPIG was provided by Shanghai Morgan Advanced Materials Co., Ltd. The graphite exhibited a porous structure with an open porosity of about 7 vol% Nickel-based superalloy (GH4169), purchased from Fushun Special Steel Shares Co., Ltd., was used as friction counterpart. The composition of GH4169 was similar to Inconel 718 alloy. The lubricating oil used was Mobil jet oil II. Mobil Jet Oil II had excellent thermal and oxidation stability, wear and corrosion protection, chemically stable, and low pour point. The main mechanical and physical parameters of both ZPIG and GH4169 are listed in Table 1.

2.2. Experiment. The ring-on-disk tests were conducted with MMW-10 friction tester. The schematic diagram of the tester was illustrated in Fig. 1(*a*). ZPIG and GH4169 were used as stationary disc and rotating ring to simulate working conditions, respectively. The inner and outer diameters of the rings were 20 mm and 26 mm. The diameter of graphite disc was 41 mm, and the thickness was 3 mm. Before test, both the disk and ring sample were treated by standard metallographic methods to ensure that their roughness was not greater than 1 μm. GH4169 ring rotated at high rotating speed as the upper sample. Graphite disk stood still immersed in the oil box as the lower sample. The load was applied by means of piston cylinder. Friction sensor recorded continuously the friction force, and COF was given after being processed by measurement system. The temperature of lubricating oil was measured by thermocouple and conducted online inspection.

To study tribological behavior of ZPIG against GH4169 under different tribological conditions in oil environment, we designed the same sliding distance test. The purpose of the test is to investigate the influence of rotating speed and load on tribological behavior. The product of rotating speed and friction time was a fixed value, and the revolutions were 36000. All tests were carried out

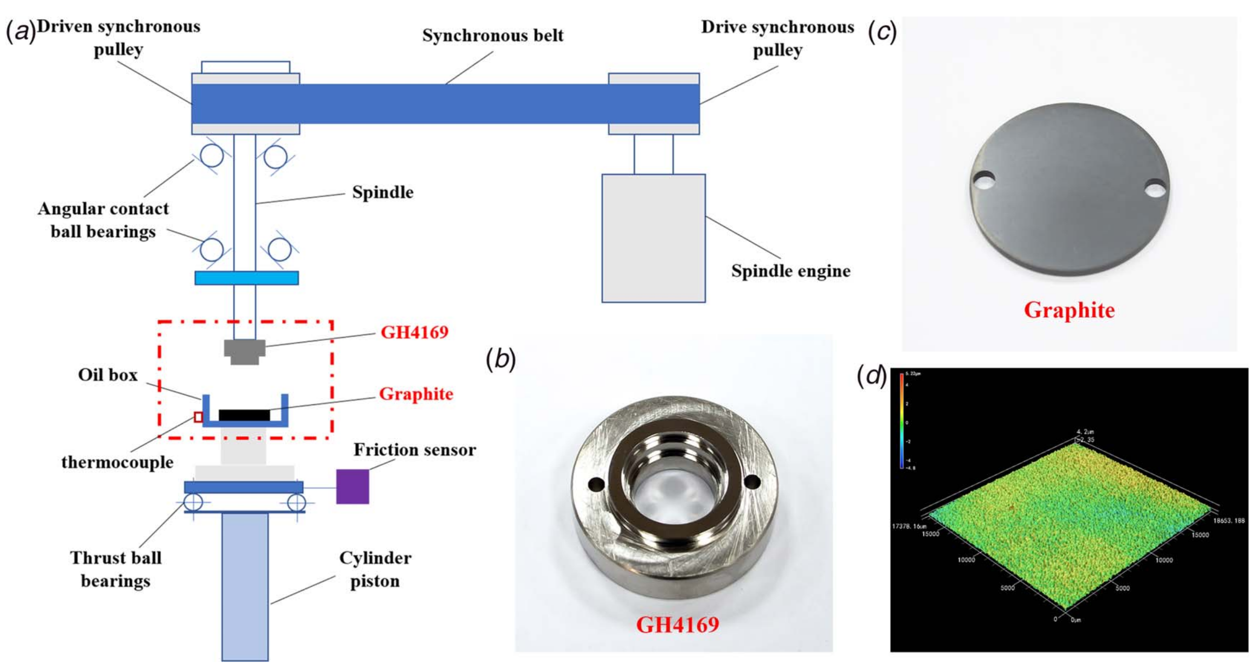

Fig. 1 (*a*) Schematic diagram of the friction tester, (*b*) optical graph of GH4169 ring, (c) optical graph of ZPIG disk, and (*d*) three-dimensional (3D) topography of polished ZPIG surface

Table 2 Experimental parameters

Load (N)	Rotating speed (rpm)	Time (h)	Temperature
500	150	4	Room temperature
	200	3	
	300	2	
	600	1	
1000	150	4	
	200	3	
	300	2	
	600	1	
2000	150	4	
	200	3	
	300	2	
	600	1	

at room temperature. The experimental parameters used in this study are given in Table 2.

2.3 Characterization. The wear loss of graphite materials under oil lubrication was very small. At the same time, there was a certain porosity inside the graphite and the immersion of lubricant would cause a small increase in the quality of graphite, so the wear loss was difficult to measure in the form of mass loss. Roughness of polished surface and wear volume were measured using a 3D measurement macroscope (Keyence VR-3200, Japan). The 3D measurement macroscope was based on the principle of white light interference technology, combined with the precise Z-direction scanning module, 3D modeling algorithm, etc. to perform noncontact scanning on the surface and establish a surface 3D image. The 3D image of surface was processed and analyzed by the system software.

Three-dimensional topographies and micrographs of wear tracks on ZPIG were acquired using a digital microscope system (Keyence VHX-6000, Japan) and scanning electron microscope (FEI Inspect F50, Hillsboro, OR). Micrographs of wear tracks on GH4169 were obtained using Keyence VHX-6000. In association with scanning electron microscopy (SEM) micrographs, component and phase composition of ZPIG were analyzed by energy dispersive spectroscopy (EDS, Oxford X-Max, UK), X-ray diffractometer (XRD), (PANalytical X'Pert Pro, Netherlands), and Raman spectrometer (WITec Alpha300, Germany).

3 Results

3.1 Structure and Properties. Figure 2(*a*) is SEM micrograph of polished ZPIG surface. White impregnated phase and pore structures are distributed on the graphite matrix. EDS and XRD analysis in Figs. 2(*c*) and 2(*d*) display graphite (matrix) and zinc phosphate (white impregnated phase) are mainly present in ZPIG. Figure 2(*b*) shows the original fracture morphology of ZPIG without grinding and polishing. Lamellar graphite can be found, and there are a certain pore structures in graphite matrix. The main purpose of adding zinc phosphate is to inhibit high-temperature oxidation of graphite materials. Pore structures are blocked by acicular or platelike zinc phosphate to form a protective cover, which is beneficial to prevent oxygen from entering the graphite interior [6,26]. However, the pore structures are not completely closed. There is still small opening, which can be confirmed by porosity in Table 1.

3.2 Coefficient of Friction and Wear-Rate. Figures 3(*a*) and 3(*b*) are the COF and wear-rate of ZPIG under different tribological conditions. The wear-rate K is calculated from Eq. (1):

$$K = \frac{V}{P_n \cdot x} \tag{1}$$

where V is the wear volume, P_n is the normal load, and x is the sliding distance.

It can be seen from Figs. 3(*a*) and 3(*b*) that the COF and wear-rate have a similar trend, which could be summarized as follows:

(1) Under the identical load condition, the COF and wear-rate at 150 rpm are both the largest, while the COF and wear-rate at

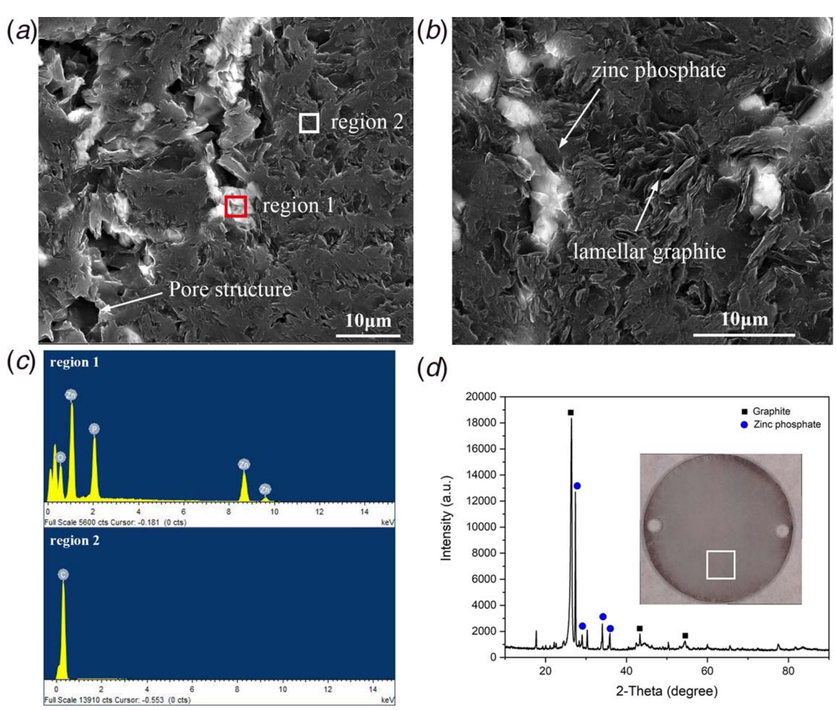

Fig. 2 (*a*) SEM micrograph of polished ZPIG surface, (*b*) SEM micrograph of ZPIG fracture, (c) EDS spectrum of region 1 and region 2, and (*d*) XRD of polished ZPIG surface

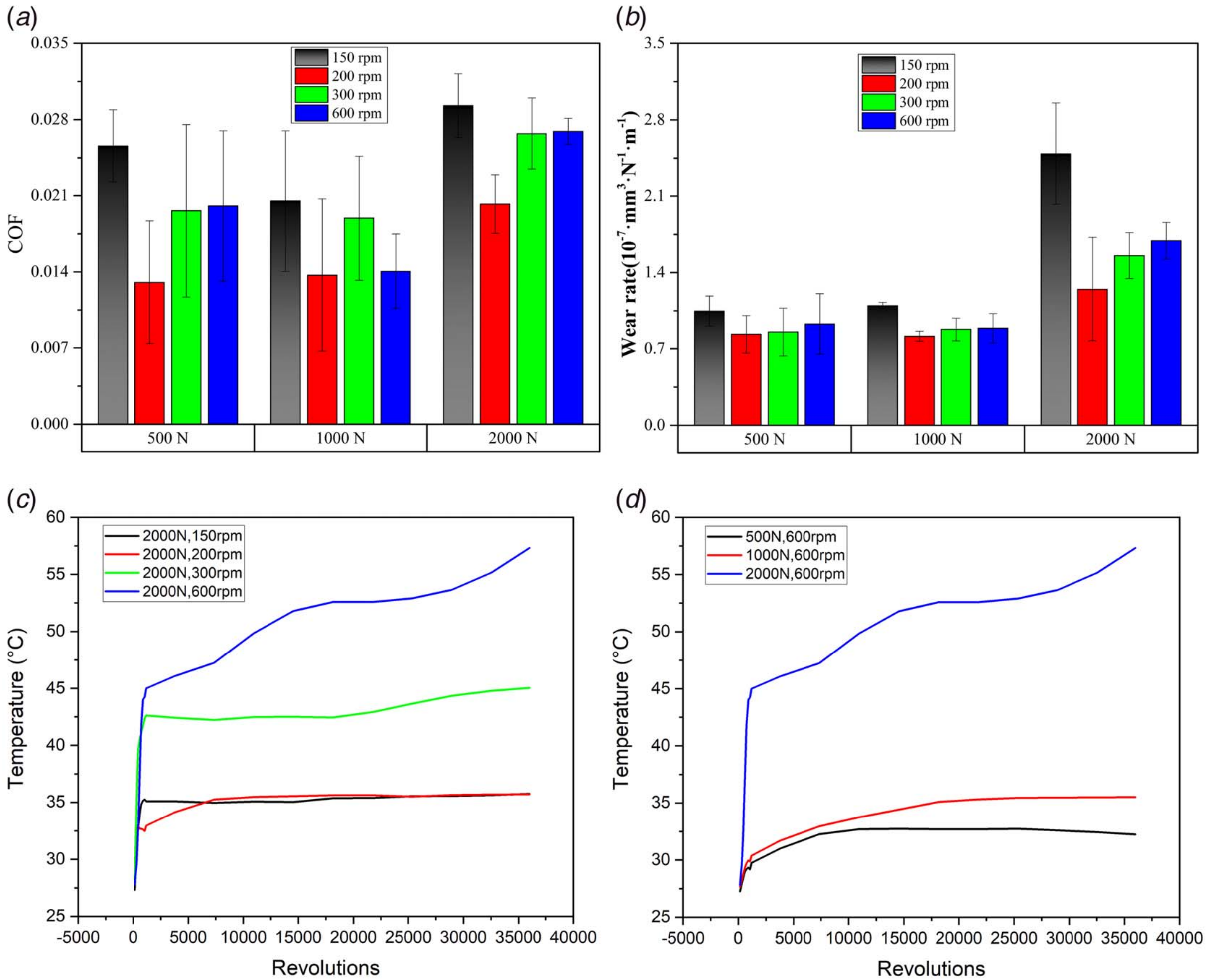

Fig. 3 (*a*) COF of ZPIG under different tribological conditions, (*b*) wear-rate of ZPIG under different tribological conditions, (*c*) relationship of oil temperature and revolutions under a load of 2000 N, and (*d*) relationship of oil temperature and revolutions at 600 rpm

200 rpm are both the smallest. When the rotating speed is greater than 200 rpm, the COF and wear-rate have a small increase.

(2) Under the identical rotating speed condition, the COF and wear-rate at 2000 N are significantly higher than other conditions. When the load is 500 N and 1000 N, the COF and wear-rate are relatively low, and the values are close.

Figure 3(*c*) shows the variation of oil temperature with revolutions under different rotating speed conditions. When the rotating speed is less than 600 rpm, the oil temperature rises rapidly (approximate linear stage) in a short time and then reaches the stable stage; and oil temperature in the stable stage is basically constant and lasts until the end of the test. The oil temperature in the stable stage at 300 rpm is significantly higher than that of 150 and 200 rpm, while oil temperature at 150 and 200 rpm is close. At 600 rpm, the oil temperature does not appear to be stable after the approximate linear stage. Instead, it has been slowly rising until the end of the test.

Figure 3(*d*) shows the variation of oil temperature with revolutions under different loads conditions. Under the identical rotating speed condition (600 rpm), the oil temperature in the stable stage is similar at 500 N and 1000 N, and the oil temperature at 1000 N is slightly higher. The final oil temperature at 2000 N is significantly higher than that of 500 N and 1000 N.

3.3 Wear Morphology. The wear morphologies of ZPIG and its counterpart-GH4169 under different tribological conditions are shown in Fig. 4, respectively. Figures 4(*a*)–4(*h*) show the wear morphologies under a fixed load but different rotating speeds. Figures 4(*g*)–4(*l*) show the wear morphologies under a fixed rotating speed but different loads.

As depicted in Figs. 4(*a*), 4(*c*), 4(*e*), and 4(*g*), the morphologies of wear tracks on ZPIG change significantly with the increase of the rotating speed. Figures 4(*b*), 4(*d*), 4(*f*), and 4(*h*) are the micrographs of the wear tracks on GH4169, and the black areas are carbon-based transfer layer. When the rotating speed is 150 rpm, uneven surface and severe damage appear in wear track on ZPIG, accompanied by spalled pits and furrows in Fig. 4(*a*). In the counterpart, continuous carbon-based transfer layer covers part of wear track on GH4169 along the sliding direction in Fig. 4(*b*). The wear track on ZPIG is smooth at 200 rpm: the furrows are the least and the spalled pits are few, like a polished surface in Fig. 4(*c*). No obvious transfer layer is found in the wear track on GH4169 in Fig. 4(*d*). The number of furrows raise and the surface fluctuation increase in wear tracks on ZPIG at 300 rpm in Fig. 4(*e*). There are many graphite particles dispersed in the wear track on GH4169, but continuous carbon-based transfer layer is not formed in Fig. 4(*f*). The typical feature of wear track on ZPIG at 600 rpm is spalled pits in Fig. 4(*g*). The wear track on GH4169 covers a certain transfer layer, while the amount is significantly less than 150 rpm in Fig. 4(*h*).

Figures 4(*g*), 4(*i*), and 4(*k*) are 3D topographies of wear tracks on ZPIG under the identical rotating speed condition. Figures 4(*h*), 4(*j*), and 4(*l*) show micrographs of the wear tracks on GH4169. When the load is 500 N, numerous thin and shallow furrows are

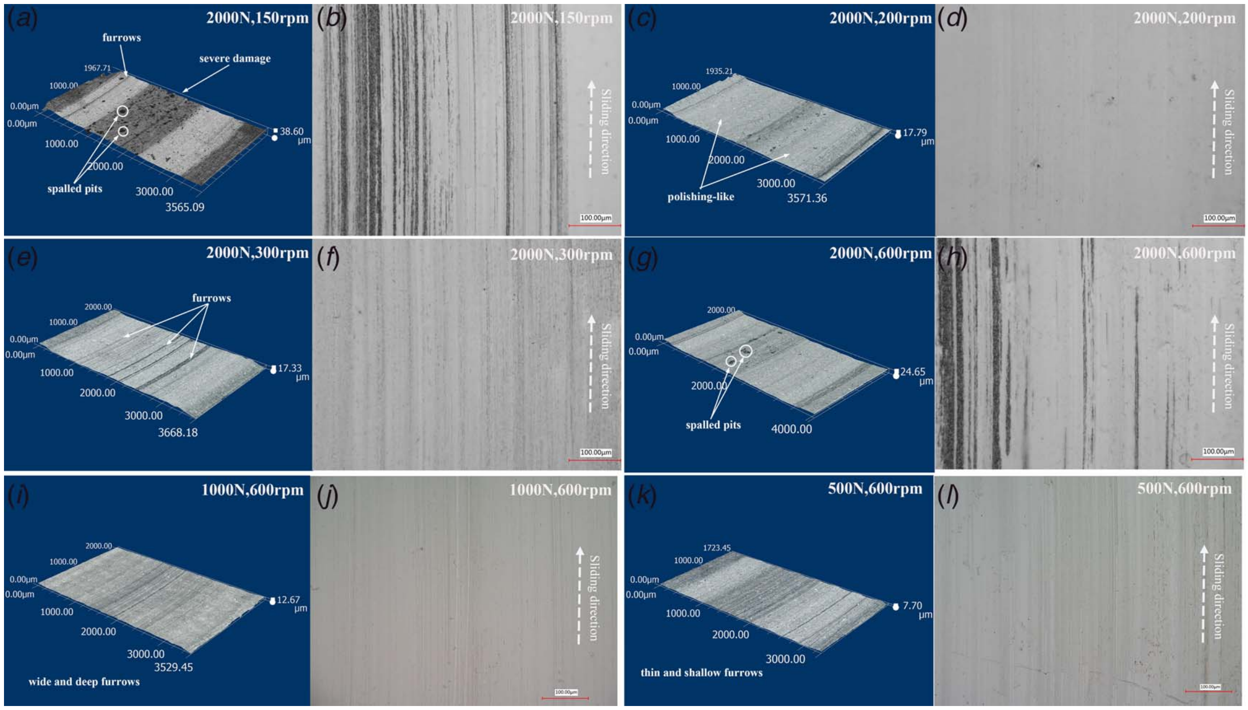

Fig. 4 Three-dimensional topographies of wear tracks on ZPIG under different tribological conditions: (*a*) 2000 N, 150 rpm, (*c*) 2000 N, 200 rpm, (*e*) 2000 N, 300 rpm, (*g*) 2000 N, 600 rpm, (*i*) 1000 N, 600 rpm, (*k*) 500 N, 600 rpm; and micrographs of the wear tracks on GH4169 under different tribological conditions: (*b*) 2000 N, 150 rpm, (*d*) 2000 N, 200 rpm, (*f*) 2000 N, 300 rpm, (*h*) 2000 N, 600 rpm, (*j*) 1000 N, 600 rpm, and (*l*) 500 N, 600 rpm

found on the ZPIG surface of wear track in Fig. 4(*k*). There is no obvious transfer layer in the wear track on GH4169 in Fig. 4(*l*). As the load increases to 1000 N, the width and depth of the furrow in wear track on ZPIG raises accordingly in Fig. 4(*i*). The situation in wear tracks on GH4169 at 1000 N is similar to 500 N, and there is no complete transfer layer formation in Fig. 4(*j*). Under a load of 2000 N, the number of furrows is greatly reduced, but there are more spalled pits and the depth of wear track is the largest in wear tracks on ZPIG in Fig. 4(*g*). At same time, the formation of the transfer layer in wear tracks on GH4169 is the best in Fig. 4(*h*). Corresponding to Figs. 3(*a*) and 3(*b*), if the carbon-based transfer layer is formed well, the COF and wear-rate is high.

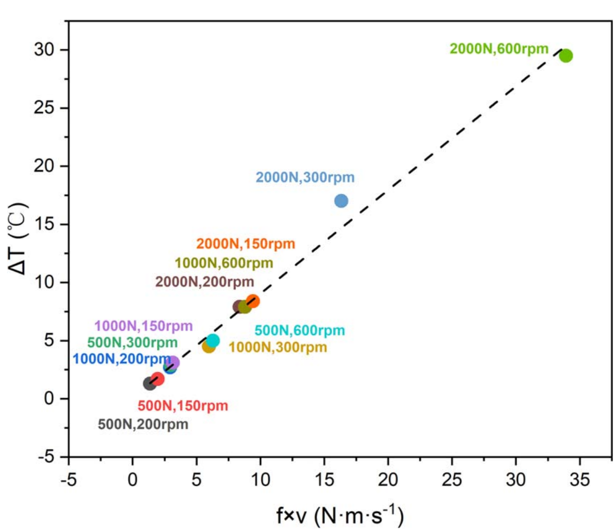

Fig. 5 Relationship of temperature rise (ΔT) and friction power (f × v) under different tribological conditions

4 Discussion

4.1 Lubrication Mechanism. Since the oil temperature has a significant effect on the viscosity of the lubricating oil, which in turn affects the lubrication and wear mechanisms, it is necessary to discuss the changes of oil temperature first. The oil temperature is related to the tribological conditions under the premise of determined the friction pair and lubricating oil. The energy required to increase the oil temperature is mainly derived from the frictional work. Figure 5 shows the relationship of temperature rise (**ΔT**) and friction power ($\boldsymbol{f \times v}$) under different tribological conditions. It can be concluded that the temperature rise is proportional to friction power. The friction power is determined by friction force ($\boldsymbol{f}$) and rotating speed ($\boldsymbol{v}$). Combined Figs. 3(*a*), 3(*c*), and 3(*d*), when the rotating speed is 600 rpm and the load is 2000 N, the friction power is the largest and the temperature rise is the highest. Under the identical load condition, the COF at 150 rpm is greater than that of 200 rpm, but the rotating speed is lower, so the temperature rise in the stable stage is basically same. The rotating speed and COF are both higher at 300 rpm, which makes the temperature rise higher. Under the identical rotating speed condition, when the load increases from 500 N to 1000 N, the COF does not change much, but the load increases twice, so the temperature rise of 1000 N is higher than 500 N.

Under oil lubrication conditions, the friction force can be described by Eq. (2) [23]:

$$f = x_l \times f_l + x_s \times f_s \quad x_l + x_s = 1 \tag{2}$$

where $\boldsymbol{f}$ is the friction force, $\boldsymbol{f_l}$ and $\boldsymbol{f_s}$ are the friction force of graphite in contact with liquids and solids, respectively; $\boldsymbol{x_l}$ and $\boldsymbol{x_s}$ are the proportions of $\boldsymbol{f_l}$ and $\boldsymbol{f_s}$, respectively. In Eq. (2), $\boldsymbol{x_l}$ and $\boldsymbol{x_s}$ are proportional to the actual area of liquid and solid contact between two surfaces. At the same time, $\boldsymbol{f_l}$ is related to the viscosity and velocity gradient of the lubricant, while $\boldsymbol{f_s}$ is determined by the contact characteristics of two solid surfaces.

In oil lubrication environment, both rotating speed and load affect the formation ability of liquid film and contact characteristics, thus affecting the lubrication and wear mechanism. When the rotating speed is greater, the more lubricating oil is squeezed into the surface of friction pair to form liquid film. Large liquid film thickness helps reduce friction force, which means that the ratio of x_l is large. When the load is greater, the liquid film is not conducive to form, which means that the ratio of x_l is small. The transfer layer on the friction counterpart-GH4169 can reflect the formation ability of liquid film. Transfer layer is the third phase with low shear strength, which is mechanically combined with the GH4169 matrix [21]; under oil lubrication conditions, it is difficult to form a complete layer due to the barrier of liquid film. When the transfer layer forms well, the thickness of the liquid film is small, and the contact area between the two solid surfaces is large, which intensifies the wear of the ZPIG.

Under the identical load condition, for 150 rpm, the formation ability of liquid film is poor due to the low speed, and there is a larger proportion of contact area between the friction pairs, so the COF and wear-rate under the tribological condition is the largest. It can be proved from Figs. 4(*b*) and 4(*d*) that a relatively complete transfer layer is formed in the wear track on GH4169 at 150 rpm, so the formation ability of liquid film is weak; while there is no obvious transfer layer at 200 rpm, the formation ability of liquid film is strong. Therefore, the COF drops rapidly when the rotating speed increases from 150 rpm to 200 rpm, and the wear-rate decreases accordingly. As the rotating speed increases further, the higher the velocity, the higher the oil temperature (Fig. 3(*c*)), which leads to a decrease in the lubrication effect (f_l increases); the shearing effect of GH4169 on graphite also raises (f_s increases). From Figs. 4(*f*) and 4(*h*), there are many graphite particles dispersed in the wear track on GH4169 at 300 rpm, but the wear track on GH4169 at 600 rpm covers a certain transfer layer. Therefore, COF and wear-rate raises slowly when the rotating speed is greater than 200 rpm, as shown in Figs. 3(*a*) and 3(*b*).

It is easy to understand that as the load increases, the lubricating oil is squeezed out from the surface of the friction pair, so the contact area of friction pair increases, and the thickness of liquid film decreases (x_l decreases). At the same time, excessive oil temperature causes the lubrication effect of lubricating oil decline (Fig. 3(*d*)). The value of f increases, which makes COF and wear-rate increase greatly from 1000 N to 2000 N. Therefore, COF and wear-rate are the largest under a load of 2000 N. Figures 4(*h*) and 4(*j*) can prove the above conclusions: the formation of the transfer layer in wear tracks on GH4169 is the best at 2000 N, but there is no complete transfer layer formation at 1000 N. Compared with 500 N, the width and depth of furrows at 1000 N increase, so the lubricating oil flow channel is formed, that is, f_l decreases. From Figs. 4(*j*) and 4(*l*), there is no obvious transfer layer at 500 N and 1000 N. As mentioned above, when load is less than 1000 N, COF and wear-rate of ZPIG is consistent, as shown in Figs. 3(*a*) and 3(*b*).

4.2 Wear Mechanism. From wear morphologies in Fig. 4, the main wear forms in wear tracks on ZPIG include severe damage, polishing-like, furrow, and spalled pit. This section discusses the formation mechanisms of these wear forms. Figure 6 shows the SEM micrographs of wear tracks under a load of 2000 N.

After being rubbed, part of wear track area produces many tiny grooves, making surface uneven as depicted in Fig. 6(*a*). The wear debris produced by cutting is easily confined. Wear debris accumulation is formed after combined action of load and shearing force, as shown in Fig. 6(*b*). The typical tribological conditions of wear debris accumulation are 2000 N, 600 rpm. In the situation, ZPIG and the counterpart-GH4169 have insufficient formation ability of liquid film, and the contact between ZPIG and GH4169 is relatively sufficient. Therefore, the existence of wear debris accumulation is usually accompanied by uneven surfaces and severe damage in Fig. 4(*a*).

The wear track is like a polished surface in Figs. 6(*c*) and 3(*d*). Under the effect of the liquid film, most area of ZPIG and GH4169 surface are separated by lubricating oil and cannot be fully contacted. The tiny bulges of ZPIG surface are prone to fracture and remove, then reaccumulate on the graphite surface to achieve a flat state through extrusion and flattening, like the polishing mechanism. At the same time, it can be found that convex phosphates are also sheared to form a smooth surface. The presence of phosphate hinders the abrasion of ZPIG. The wear mechanism is representative at 2000 N, 200 rpm in Fig. 4(*c*). In this situation, the formation ability of the liquid film is strong, which leads to a lower wear-rate.

A typical ploughing wear can be found in Fig. 4(*e*). There are inevitably larger hard phase protrusions on surface of GH4169. These hard phase protrusions are embedded in graphite surface under the action of normal load. During sliding process, the hard phase protrusions plough graphite surface, which is a fracture mechanism, thus forming furrows. From Figs. 6(*e*) and 3(*f*), it can be found that lamellar graphite structures expose inside produced by ploughing action, and pore structures exist in furrows, cut zinc

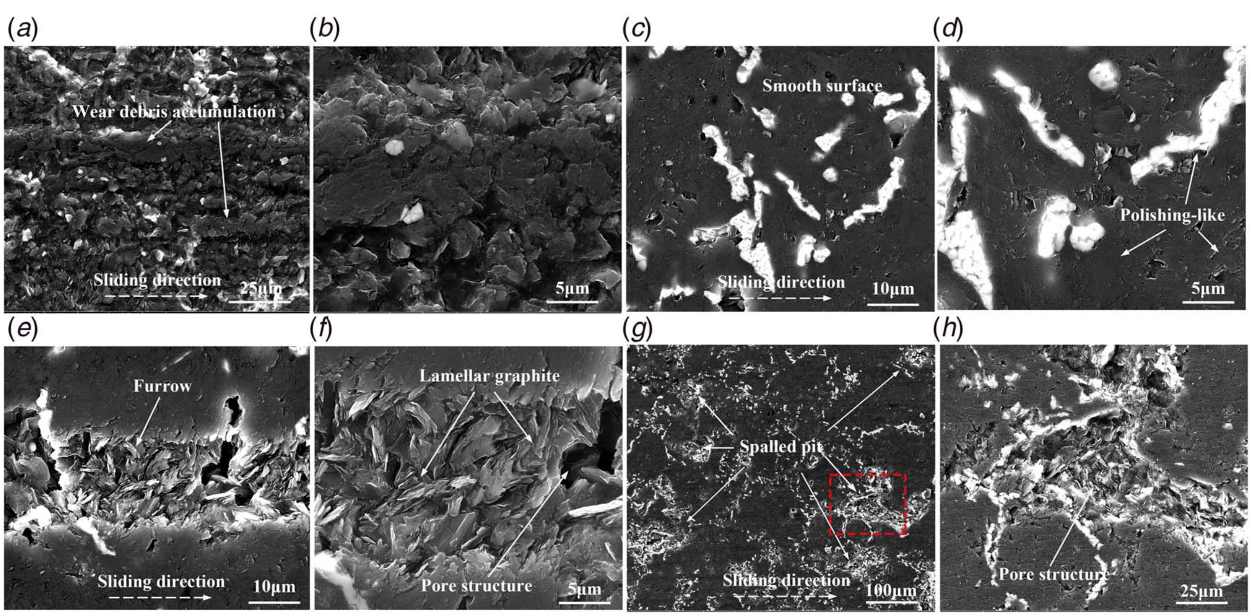

Fig. 6 SEM micrographs of wear tracks under a load of 2000 N: (*a*) and (*b*) 150 rpm, (c) and (*d*) 200 rpm, (*e*) and (*f*) 300 rpm, and (*g*) and (*h*) 600 rpm

phosphate also found. Combined with Figs. 4(*e*), 4(*i*), and 4(*k*), when the furrow mechanism is formed, the thickness of the liquid film is thinner, but the lubrication effect is not bad and the wear-rate is relatively low.

Observing Figs. 4(*a*) and 4(*g*), there are certain spalled pits on surface of ZPIG. Through the SEM micrographs Figs. 6(*g*) and 6(*h*) of spalled pits, there is a large amount of zinc phosphate in spalled pit. The area where the spalled pits are located is the large pore structure in ZPIG. Due to the large pore structure, mechanical properties are poor and it is easy to induce cracks. Crack expands under action of shearing force, resulting in spalled pit, as depicted in Fig. 4(*a*). In the meantime, under condition of high load and rotating speed, the flowrate of liquid film is very high, and load generated by liquid film also accelerates generation and expansion of spalled pits, as shown in Fig. 4(*g*). Therefore, spalled pits usually appear in high-speed or heavy-load conditions, and they grow up due to the action of shearing force or oil pressure.

Raman spectra of ZPIG under different tribological conditions are shown in Fig. 7. Three characteristic peaks exist in the Raman spectrum of ZPIG: D peak at 1350 cm^{-1}, G peak at 1580 cm^{-1}, and two-dimensional (2D) peak at 2700 cm^{-1}. The D (Defect) peak is related to the defects and represents the disordered state of carbon. The G (graphite) peak reflects the ideal graphite vibration mode with E_{2g} symmetry which corresponds to the bond expansion of in-plane vibration of sp2 atom. The G peak represents the order of graphite structure, and its peak position is consistent with natural graphite, so it is generally called ordered carbon or graphitic carbon. 2D peak is described as characteristics of undisturbed or highly ordered graphite lattices, which also reflect the ordered structure of graphite [27,28].

The intensity ratio of I_D/I_G, can be used to measure degree of graphitization of the graphite material [29,30]. The smaller ratio, the more complete the crystallization, and the higher degree of graphitization of material. As depicted in Fig. 7, ZPIG is basically composed of lamellar graphite with a high degree of graphitization because the intensity of G peak is higher than D peak. The intensity of the D peak is basically identical under different conditions, so the ratio of I_D/I_G could be reflected by the intensity of the G peak. The intensity of the G peak is the lowest at 200 rpm. Under the polishing-like mechanism, the disorder of the ZPIG increases and the intensity of G peak decreases. In this situation, the polishing-like mechanism is dominant and the wear-rate of ZPIG is smaller, which is consistent with Figs. 4(*c*), 6(*c*), and 6(*d*). The intensity of the G peak is high at 300 rpm and 600 rpm. The proportion of furrow and spalled pit has increased significantly on the worn surface in Figs. 4(*e*) and 4(*g*). More lamellar graphite structures are exposed inside in Figs. 6(*f*) and 6(*h*), which increase the intensity of G peak. As shown in Fig. 4(*a*), the wear debris accumulation accounts for a larger proportion. Lots of wear debris accumulate and reorganize on the graphite surface in Figs. 6(*a*) and 6(*b*). Therefore, the intensity of G peak is in the middle position at 150 rpm.

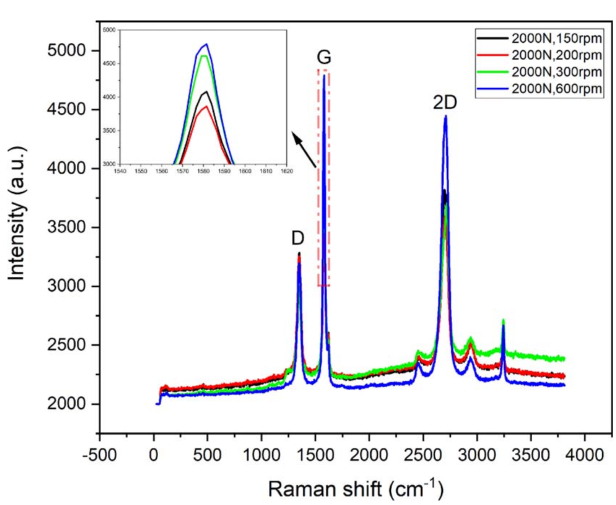

Fig. 7 Raman spectra of ZPIG under different tribological conditions. Insets are the magnification of G bands.

By summing up the above conclusions, it can be found that the wear of ZPIG under oil lubrication conditions is dominated by abrasive wear, and material removal is achieved through the fracture mechanism. Zinc phosphate can hinder the wear of graphite matrix to a certain extent. At the same time, the third phase graphite debris formed can be stored in a smaller pore structure to achieve the effect of reducing wear.

Wear mechanism is mainly manifested as: wear debris accumulation (Figs. 6(*a*) and 6(*b*)); polishing-like mechanism (Figs. 6(*c*) and 6(*d*)); furrow (Figs. 6(*e*) and 6(*f*)); spalled pit (Figs. 6(*g*) and 6(*h*)). The lubrication mechanism has an important influence on the wear mechanism. When the lubrication effect is good, the wear mechanism is mainly polishing-like mechanism and furrow, resulting in lower COF and wear-rate. When the lubrication effect is poor, the proportion of wear debris accumulation and spalled pit increases, resulting in higher COF and wear-rate.

5 Conclusions

(1) In oil-lubricated environment, zinc phosphate impregnated graphite exhibits good friction and wear performance at 200 rpm under any load conditions. When rotating speed is lower than 200 rpm, coefficient of friction and wear-rate increase greatly; as rotating speed higher than 200 rpm, coefficient of friction and wear-rate both increase slightly.

(2) Zinc phosphate impregnated graphite shows smaller coefficient of friction and wear-rate under a load of 1000 N. The COF and wear-rate change little as the load increases from 500 N to 1000 N; when the load reaches 2000 N, the coefficient of friction and wear-rate increase significantly with the raise of the load.

(3) The lubrication mechanism of zinc phosphate impregnated graphite is related to contact characteristics of solid surfaces and formation ability of liquid film, thereby affecting the COF, wear-rate, and oil temperature. The transfer layer of the friction counterpart can reflect the contact characteristics of two solid surfaces.

(4) The wear mechanism of zinc phosphate impregnated graphite under oil lubrication conditions is dominated by abrasive wear, and material removal is achieved through the fracture mechanism. Wear mechanism is mainly manifested as: polishing-like mechanism; furrow; wear debris accumulation; spalled pit. Lubrication mechanism has an important influence on the wear mechanism. The wear mechanism is mainly polishing-like mechanism and furrow under good lubrication effect, resulting in lower COF and wear-rate. The proportion of wear debris accumulation and spalled pit increases under poor lubrication effect, resulting in higher COF and wear-rate.

Conflict of Interest

There are no conflicts of interest.

Data Availability Statement

The datasets generated and supporting the findings of this article are obtainable from the corresponding author upon reasonable request. The authors attest that all data for this study are included in the paper. No data, models, or code were generated or used for this paper.

References

[1] Blau, P. J., and Martin, R. L., 1994, "Friction and Wear of Carbon Graphite Materials Against Metal and Ceramic Counterfaces," Tribol. Int., **27**(6), pp. 413–422.

[2] Williams, J. A., Morris, J. H., and Ball, A., 1997, "The Effect of Transfer Layers on the Surface Contact and Wear of Carbon-Graphite Materials," Tribol. Int., **30**(9), pp. 663–676.

[3] Zhu, Z. G., Bai, S., Wu, J. F., Xu, L., Li, T., Ren, Y., and Liu, C., 2015, "Friction and Wear Behavior of Resin/Graphite Composite Under Dry Sliding," J. Mater. Sci. Technol., **31**(3), pp. 325–330.

[4] Jin, J., Peng, X. D., Jiang, J. B., Meng, X. K., and Zhao, W. J., 2020, "Frictional Characteristics of Impregnated Graphite With Different Graphitization Degree Versus Chromium Stainless Steel Under Varying PV Values," Tribol. Int., **146**, p. 106063.

[5] Lebeck, A. O., 1991, *Principles and Design of Mechanical Face Seals*, Wiley, New York.

[6] Lee, Y. J., and Radovic, L. R., 2003, "Oxidation Inhibition Effects of Phosphorus and Boron in Different Carbon Fabrics," Carbon, **41**(10), pp. 1987–1997.

[7] Savchenko, D. V., Serdan, A. A., Morozov, V. A., Van Tendeloo, G., and Ionov, S. G., 2012, "Improvement of the Oxidation Stability and the Mechanical Properties of Flexible Graphite Foil by Boron Oxide Impregnation," New Carbon Mater., **27**(1), pp. 12–18.

[8] Lin, Y. F., Liu, T. L., Wang, J., Lu, J. N., Dong, X. R., and Feng, X. W., 2020, "Fabrication and Oxidation Resistance Behavior of Phosphate/Borate Impregnation for Graphite," Surf. Coat. Technol., **389**, p. 125632.

[9] Song, Y. Z., Zhai, G. T., Song, J. R., Li, G. S., Shi, J. L., Guo, Q. G., and Liu, L., 2006, "Seal and Wear Properties of Graphite From MCMBs/Pitch-Based Carbon/Phenolic-Based Carbon Composites," Carbon, **44**(13), pp. 2793–2796.

[10] Hirani, H., and Goikar, S. S., 2009, "Formation of Transfer Layer and Its Effect on Friction and Wear of Carbon-Graphite Face Seal Under Dry, Water and Steam Environments," Wear, **266**(11–12), pp. 1141–1154.

[11] Gulevskii, V. A., Antipov, V. I., Kolmakov, A. G., Vinogradov, L. V., Lazarev, E. M., Mukhina, Y. E., and Gordeev, A. S., 2012, "Designing of Copper-Based Alloys for the Impregnation of Carbon-Graphite Materials," Russ. Metall., **2012**(3), pp. 258–261.

[12] Bernal, J. D., 1924, "The Structure of Graphite," Proc. R. Soc. London, Ser. A, **106**(740), pp. 749–773.

[13] Bragg, W. H., 1928, *An Introduction to Crystal Analysis*, G. Bell and Sons, Limited.

[14] Bryant, P. J., Gutshall, P. L., and Taylor, L. H., 1964, "A Study of Mechanisms of Graphite Friction and Wear," Wear, **7**(1), pp. 118–126.

[15] Savage, R. H., 1948, "Graphite Lubrication," J. Appl. Phys., **19**(1), pp. 1–10.

[16] Savage, R. H., and Schaefer, D. L., 1956, "Vapor Lubrication of Graphite Sliding Contacts," J. Appl. Phys., **27**(2), pp. 136–138.

[17] Bollmann, W., and Spreadborough, J., 1960, "Action of Graphite as a Lubricant," Nature, **186**(4718), pp. 29–30.

[18] Spreadborough, J., 1962, "The Frictional Behaviour of Graphite," Wear, **5**(1), pp. 18–30.

[19] Clark, W. T., and Lancaster, J. K., "Breakdown and Surface Fatigue of Carbons During Repeated Sliding," Wear, **6**(6), pp. 467–482.

[20] Lancaster, J. K., 1975, "Transitions in Friction and Wear of Carbons and Graphites Sliding Against Themselves," ASLE Trans., **18**(3), pp. 187–201.

[21] Jones, G. A., 2004, "On the Tribological Behaviour of Mechanical Seal Face Materials in Dry Line Contact—Part I. Mechanical Carbon," Wear, **256**(3–4), pp. 415–432.

[22] Jones, G. A., 2004, "On the Tribological Behaviour of Mechanical Seal Face Materials in Dry Line Contact—Part II. Bulk Ceramics, Diamond and Diamond-Like Carbon Films," Wear, **256**(3–4), pp. 433–455.

[23] Zhang, G. L., Liu, Y., Guo, F., Liu, X. F., and Wang, Y. M., 2017, "Friction Characteristics of Impregnated and Non-Impregnated Graphite Against Cemented Carbide Under Water Lubrication," J. Mater. Sci. Technol., **33**(10), pp. 1203–1209.

[24] Zhang, G. L., Liu, Y., Wang, Y. C., Guo, F., Liu, X. F., and Wang, Y. M., 2017, "Wear Behavior of WC-Ni Sliding Against Graphite Under Water Lubrication," J. Mater. Sci. Technol., **33**(11), pp. 1346–1352.

[25] Zhao, J., Li, Q. Z., Li, S. X., Li, S. C., Chen, G. Y., Liu, X. H., He, Y. Y., and Luo, J. B., 2020, "Influence of a Carbon-Based Tribofilm Induced by the Friction Temperature on the Tribological Properties of Impregnated Graphite Sliding Against a Cemented Carbide," Friction, **9**(4), pp. 686–696.

[26] Wu, X. X., and Radovic, L. R., 2006, "Inhibition of Catalytic Oxidation of Carbon/Carbon Composites by Phosphorus," Carbon, **44**(1), pp. 141–151.

[27] Cuesta, A., Dhamelincourt, P., Laureyns, J., Martínez-Alonso, A., and Tascón, J. M. D., 1994, "Raman Microprobe Studies on Carbon Materials," Carbon, **32**(8), pp. 1523–1532.

[28] Sadezky, A., Muckenhuber, H., Grothe, H., Niessner, R., and Pöschl, U., 2005, "Raman Micro Spectroscopy of Soot and Related Carbonaceous Materials: Spectral Analysis and Structural Information," Carbon, **43**(8), pp. 1731–1742.

[29] Tuinstra, F., and Koenig, J. L., 1970, "Raman Spectrum of Graphite," J. Chem. Phys., **53**(3), p. 1126–1130.

[30] Lafon-Placette, S., Delbé, K., Denape, J., and Ferrato, M., 2015, "Tribological Characterization of Silicon Carbide and Carbon Materials," J. Eur. Ceram. Soc., **35**(4), pp. 1147–1159.